

Double-PFG MR imaging of the CNS: probing underlying grey matter microstructure

N. Shemesh¹, D. Barzany², O. Sadan³, Y. Zur⁴, D. Offen⁵, Y. Assaf², and Y. Cohen¹

¹School of Chemistry, Tel Aviv University, Tel Aviv, Israel, ²Department of Neurobiology, Tel Aviv University, Israel, ³Department of Neurology, Tel-Aviv Medical Center, Tel Aviv University, Israel, ⁴GE Healthcare, Israel, ⁵Laboratory of Neurosciences, Felsenstein Medical Research Center, Department of Neurology, Rabin Medical center and Tel Aviv University, Israel

Introduction. Single-Pulsed-Field-Gradient (s-PFG) MR methods such as diffusion tensor imaging (DTI)¹ and q-space imaging² have become the methods of choice for characterizing white matter tissues in central nervous system (CNS) tissues owing to their ability to portray diffusion anisotropy in coherently organized structures having ensemble anisotropy (eA). However, conventional s-PFG methodologies are extremely limited when anisotropic compartments are randomly oriented (such as grey matter); in these cases, diffusion appears isotropic in s-PFG and the underlying microstructural information is completely lost. The angular double-PFG (d-PFG) experiment³, which makes use of two of the inherently unique parameters of d-PFG, namely the angle ψ between the gradients and the mixing time (t_m), is emerging as a powerful means to characterize microstructure even in such scenarios since it can uniquely depict compartment shape anisotropy⁴ and microscopic anisotropy⁵⁻⁷ (μA), therefore providing a promising approach towards characterization of underlying grey matter microstructure. Recently, angular d-PFG spectroscopy experiments were performed on a variety of specimens ranging from coherently organized microcapillaries⁸ to randomly oriented pores⁹ and even grey and white matter tissues¹⁰, showing the possibility of obtaining unique microstructural information.

Aims. To explore the possibility of revealing microstructural features within grey matter tissues using d-PFG MRI.

Methods. All experiments were performed on a 7T Bruker Biospec equipped with a gradient system capable of producing up to 40 G/cm in all directions. A double-Pulsed-Gradient-Spin-Echo (d-PGSE) MRI sequence with EPI readout was written in-house. First, the d-PFG MRI was performed on a phantom comprised of microcapillaries having inner diameter of $20 \pm 1 \mu m$ that were aligned with their main axis pointing towards the z-direction. The in-plane resolution was 280 μm isotropic, and the slice thickness was 15 mm. Experiments were also performed on ex-vivo rat brain, where the in-plane resolution was 141 μm isotropic, and the slice thickness was 1.2 mm. Further experiments were performed on pig spinal cord, where the in-plane resolution was 100 μm isotropic, and the slice thickness was 2 mm. For the phantom, $\Delta_1 = \Delta_2 = 55$ ms, $\delta_1 = \delta_2 = 2$ ms, and $t_m = 2.2$ ms were selected, and the experiment was performed at $2q = 510$ cm^{-1} . For the spinal cord $\Delta_1 = \Delta_2 = 25$ ms,

$\delta_1 = \delta_2 = 4$ ms, and $t_m = 4.2$ ms were used. For the rat brain, the same parameters were used except $\Delta_1 = \Delta_2 = 20$ ms. These experiments were performed at $2q = 1090$ cm^{-1} . The angular d-PFG experiment⁸ was performed in the X-Y plane and the angle ψ was incremented in 30° steps between 0° and 360°. The $E(\psi)$ images were co-registered and then all of the images were normalized to a reference image $E_{ref} = ((E(\psi=0^\circ) + E(\psi=360^\circ))/2)$, yielding normalized $E(\psi)$ images. To search for patterns within the 13 ψ values, multiparametric clustering was performed using the kmeans clustering algorithm as previously described¹¹.

Results and Discussion. Figure 1 shows the normalized data ($E(\psi)/E_{ref}$) of the d-PFG MRI images of the phantom. The expected angular profile for coherently organized fibers when the experiment is conducted in the X-Y plane⁸ is an increase in $E(\psi)$ up to $\psi = 180^\circ$ and then a decrease up to $\psi = 360^\circ$. The images along the different ψ values robustly show the expected pattern. The colored image shows the clustering, demonstrating a single pattern within the phantom. The normalized $E(\psi)$ plot of the pattern (right panel) clearly shows the expected angular profile. Figure 2 shows the raw $E(\psi)$ data from the rat brain. Note that when anisotropic compartments are randomly oriented, the $E(\psi)$ plots at short t_m manifest modulations that are dependent on compartment eccentricity and on μA ^{4,9}. These modulations can be clearly observed even in the raw data (see areas marked with arrows in the $\psi = 0^\circ$ image for example). In the cortex, a decrease in $E(\psi)$ can be easily observed up to $\psi = 90^\circ$, with a subsequent increase up to $\psi = 180^\circ$. Then, this behavior is mirrored up to $\psi = 360^\circ$, as expected⁹. Figure 3A shows a synthesized Paxinos and Watson atlas with the map of the clusters, showing diversity of $E(\psi)$ plots within different grey matter regions. Figure 3B shows four representative $E(\psi)$ plots from cortical clusters. The brown, blue and cyan clusters show marked differences, demonstrating that water is diffusing in randomly compartments of different eccentricities; the orange clusters show characteristics of more coherent ordering, like one would expect from areas with more white matter contribution. These findings show underlying microstructural heterogeneity of the cortex. While there is no reason to expect that these data will exactly correspond to different functional regions (since they only convey microstructural differences), there seems to be some similarities to the Paxinos and Watson atlas, especially in the more lateral cortex. Figure 3C shows data from the striatum. Here, although the clustering algorithm finds different behaviors, the $E(\psi)$ plots are quite similar to one another, suggesting little microstructural heterogeneity at this slice of the striatum. Of course, this could be to some extent a manifestation of partial volume effects, and it is highly likely that signal from more anterior parts, where the striatum is more uniform, contribute substantially to the similarity of the $E(\psi)$ plots. Histological studies are underway to corroborate the d-PFG MRI findings. Similar observations were made in the grey matter of spinal cords (data not shown).

Conclusions. These findings suggest that d-PFG MRI may become a very useful means to characterize grey matter underlying microstructure.

Acknowledgments. Y.C., N.S., Y.A. and D.B. were partially supported by the CONNECT consortium administered by the European commission under framework package 7.

References. [1] Bassar PJ et al., Biophys. J. 1994, 66:259. [2] Cohen Y and Assaf Y, NMR Biomed 2002, 15:516. [3] Mitra PP, Phys. Rev. B, 1995, 51:15074. [4] Özarslan E, J. Magn. Reson. 2009, 199:56. [5] Özarslan E, Bassar PJ, J. Chem. Phys. 2008, 128:154511. [6] Komlosh ME et al., Magn. Reson. Med. 2007, 59:803. [7] Koch MA and Finsterbusch J, Magn. Reson. Med. 2008, 60:90. [8] Shemesh et al., NMR Biomed 2010, 23:757. [9] Shemesh N et al., J. Chem. Phys. 2010, 133:044705. [10] Shemesh N and Cohen Y, Magn. Reson. Med., 2010, accepted for publication. [11] Yovel Y and Assaf Y, Neuroimage 2007, 35:58.

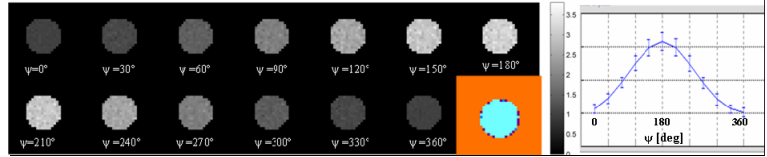


Figure 1. Double-PFG MRI of the phantom. Normalized $E(\psi)$ images are shown.

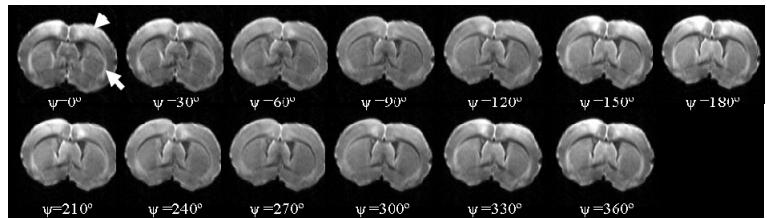


Figure 2. Double-PFG MRI of the rat brain – raw data.

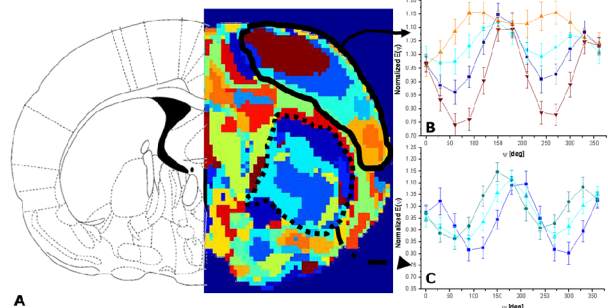


Figure 3. (A) A synthesized Paxinos and Watson atlas and cluster map. (B) Normalized $E(\psi)$ plots for four selected clusters in the cortex. (C) Normalized $E(\psi)$ plots for clusters in the striatum.

Figure 3A shows a synthesized Paxinos and Watson atlas and cluster map. (B) Normalized $E(\psi)$ plots for four selected clusters in the cortex. (C) Normalized $E(\psi)$ plots for clusters in the striatum.